Optical force sensing – validation of a 1-ray model

Application Note

Published by ams-OSRAM AG
Tobelbader Strasse 30,
8141 Premstaetten Austria
Phone +43 3136 500-0
ams-osram.com

Optical force sensing – validation of a 1-ray model

Application Note No. AN001067

Valid for:
SFH 4053, SFH 5721

Abstract

This note shares measurement results and validity assessment of a simple one-ray model for optical force sensing.

It shows that:

- The model presents a useful analysis and prediction tool for an optical force sense configuration with a side-by-side emitter-detector under ceiling combination
- ams OSRAM's SFH 4053 and SFH 5721 enable low profile and low power optical force sensing and form a compelling alternative to capacitive touch sensors
- Even at single mA SFH 4053 bias currents, optical force depression uncertainty can be sub-micrometer

Table of contents

1 Introduction

Optical force sensing uses a light emitter and a light detector (in our case SFH 4053 and SFH 5721, respectively) located side-by-side in a coplanar fashion underneath a flexible and reflecting surface. This allows the sensor to measure how deeply the surface is depressed.

This note shares some typical measurement results to check the validity of an extremely simple one-ray model. We will show you that:

- Despite this model's simplicity, it allows an accurate analysis and prediction of an optical emitter-detector under ceiling geometry as in figure 1 (sections 3.4 through 3.6)
- Components SFH 4053 and SFH 5721 and a ceiling height range of less than 3 mm allow for very low profile and low power optical force sensing and form a compelling alternative to capacitive touch implementations (section 3.7.6)
- Even at single mA SFH 4053 bias currents, one sigma ceiling depression uncertainty can be sub-µm, contingent on careful selection of SFH 5721 gain and integration time (sections 3.7.2 through 3.7.5)
- For diffuse ceilings there are two regions two choose from favoring either sensitivity or dynamic range (sections 3.7.2 through 3.7.5)
- Measurements show system's Gaussian statistics interpretation is allowed (section 4)

2 Physical model

This chapter presents a model of an optical force sensor. We will introduce the key characteristics and equations to understand the system and predict new builds' behavior.

2.1 Simplifications

The model makes several simplifications:

- The emitter is a point source, and the sensor is a point sink. The model takes the centers of the respective die as start and end points of the optical ray of interest
- The emitter, the detector and the diffuse ceiling all show Lambertian behavior, resulting the cos(φ) terms in Equation 1
- The behavior is sufficiently described by following one optical ray from the emitter to the detector which reduces in radiation intensity I(φ,d) according to $1/d^2$, d being its length
- The ceiling is fully reflective, flat and specular (mirror-like) or diffusing, and it reflects the one ray of interest from emitter to sensor with equal incident and exiting angles
- Crosstalk (light on the sensor not originating from the sensor via the ceiling) is ignored in the equations, but in actuality is a significant contributor to the sensor readout. In measurements it is separately and subtracted from the output value for I(h)'s calculation
- Absolute values of emitter output power, ceiling reflectivity and others that are of influence on the output signal's value are not within scope of this note, and addressed by I_0 in the equations and curve-fitting

2.2 Equations

Figure 1 depicts components 1 and 2 with lateral spacing s (vertical center lines) and heights t_1 and t_2 (horizontal center lines) between their centers A and D. We have taken component 1 to be the emitter and the detector as component 2, just a matter of convenience.

The diagram also shows component 2 mirrored in the ceiling, the mirrored objects are dotted. The mirror of D (center of component 2) is C. This allows constructing the light ray (red) from A to D by drawing a line from A to C, and where it intersects with the ceiling at E, drawing a line to D.

Figure 1: Diagram for derivation of equations

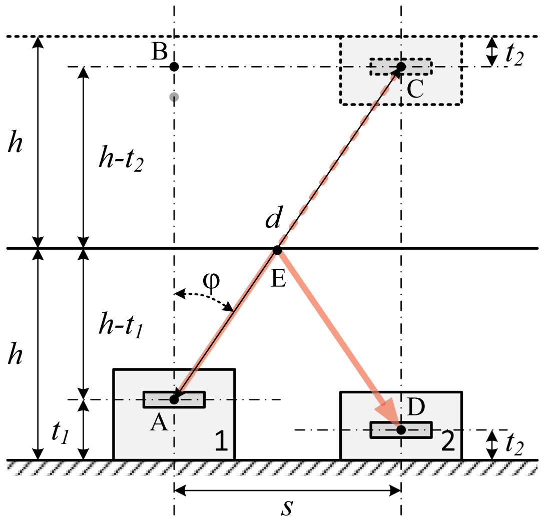

Note that distance BC is s and AB = $(h\text{-}t_1 + h\text{-}t_2) = (2h\text{-}t_1\text{-}t_2) = (2h\text{-}t)$, where we define $t = t_1 + t_2$. We can now determine d and φ from the triangle ABC: $d^2 = (2h\text{-}t)^2 + s^2$ and $\cos(\varphi) = (2h\text{-}t)/d$

Under the assumptions that we have

- A Lambertian emitter $I(\varphi) \propto \cos(\varphi)$
- A Lambertian detector $I'(\varphi) \propto \cos(\varphi)$
- Radiant power density as ∝ distance^{-2}
- Specular ("mirror-like", non-diffuse) ceiling

the detected radiant intensity on the detector becomes as Equation 1, in which I_0 is a constant to account for emitter output power, value of reflectivity and other minor scalars of relevance.

Equation 1: Physics

$$I = \frac{\cos(\varphi) \cdot \cos(\varphi)}{d^2} I_0$$

Using the geometry equations from Figure 1 we can rewrite Equation 1 as:

Equation 2: Model

$$I(h) = \frac{(2h - t)^2}{((2h - t)^2 + s^2)^2} I_0$$

Figure 2: The impact of the $cos^2(\varphi)$ and $1/d^2$ terms in the equation 1

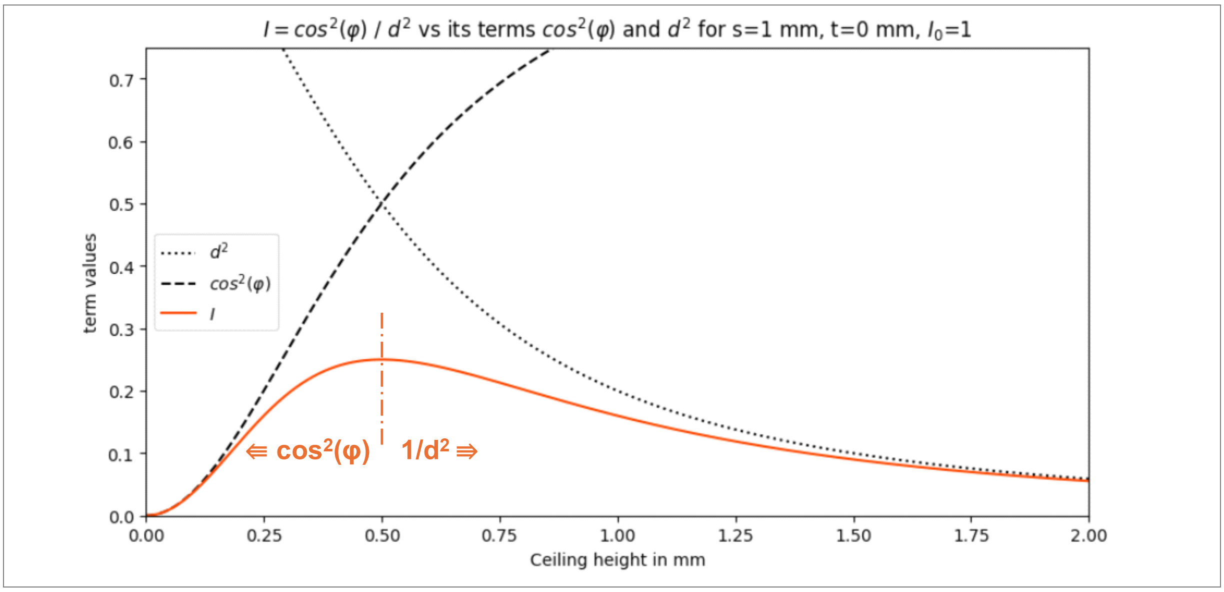

The peak of Equation 1 is caused by the $cos^2(\varphi)$ term increasing and the $1/d^2$ term decreasing with ceiling height. To the left of the peak the angle term dominates, to the right the distance term. Worthy to note is that the $cos^2(\varphi)$ term is steeper than the $1/d^2$ term.

3 Measurements

3.1 Set-up

Figure 3 shows the measurement set-up used. It includes:

- 3 Thorlabs LTS150 translation stages with 150 mm range and ±5 µm accuracy (lower part of figure) to computer control the
  - Spacing between emitter and receiver
  - Ceiling height between the reflectors and the emitter and receiver
  - Reflection material (specular and diffuse)
- 2 PCBs with ams OSRAM SFH 4053 emitter and SFH 5721 receiver each on a small nose extension (right upper part of figure) to allow close proximity between the emitter and receiver, and unobstructed proximity between components and ceiling
  - The tip of the SFH 4053 PCB is covered by a very small piece of adhesive aluminum tape to limit the amount of crosstalk (left-upper part of figure)
- 2 materials attached to the ceiling of different reflection natures, Aluminum tape for a specular reflection and Teflon tape for a diffuse one (lower right)
- An ESP32 DEVKIT V1 micro-controller board to manage SFH 5721 receiver (via I²C) from the personal computer (via USB) running the control software

Figure 3: Measurement set-up

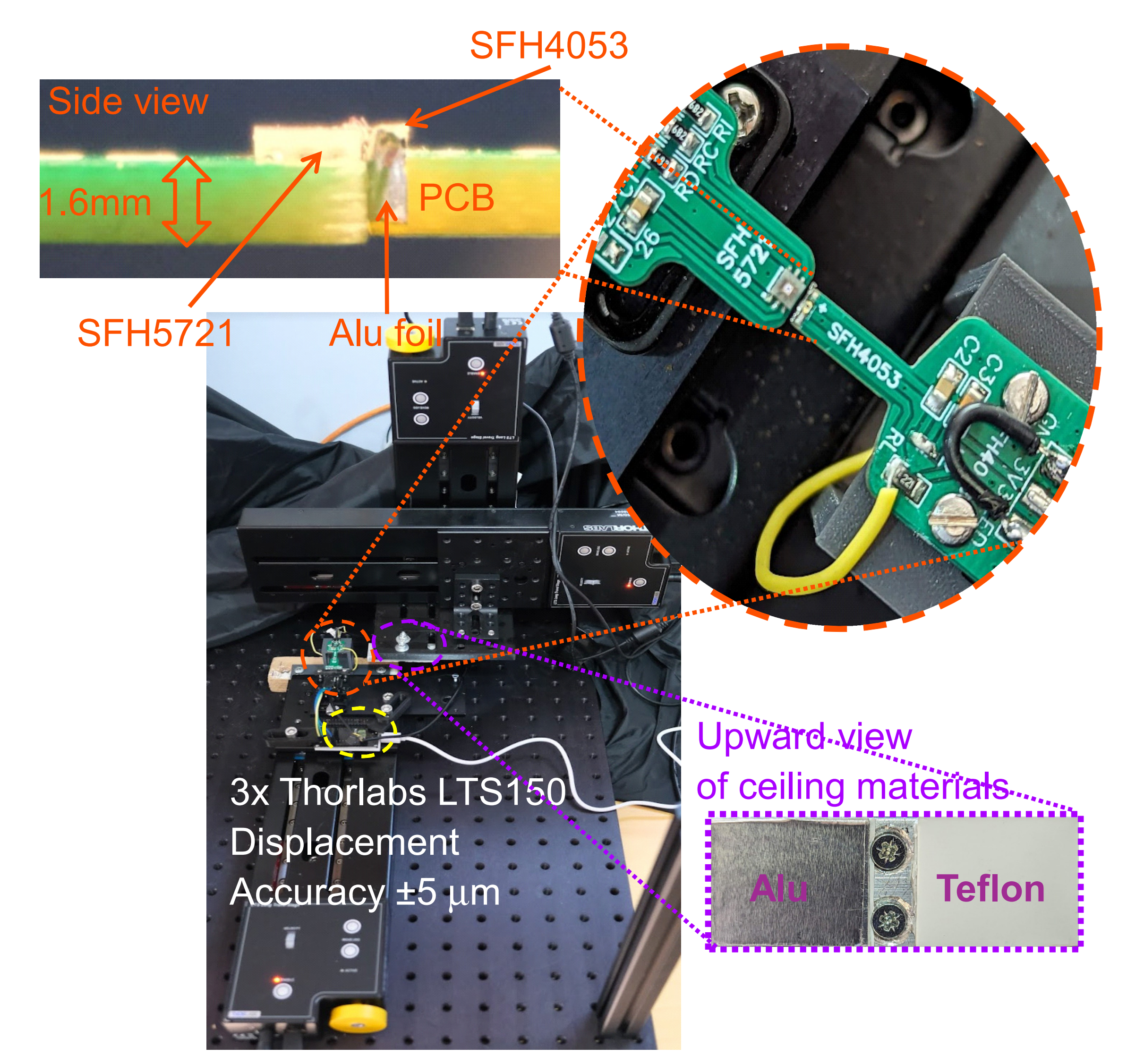

3.2 SFH 5721 and SFH 4053 key settings

Let’s review the relevant SFH 5721 characteristics and settings as they will show up in the results below.

- Counts; unitless SFH 5721 output value linear to the detector’s irradiance in µW/cm²
- Integration time t_{int}; the time window in which counts are accumulated
- Analog gain; optical front-end setting to optimally match signal range to ADC

For the SFH 4053 only its bias current setting will show up in the results below.

3.3 Estimation of t and s from datasheet and PCB

Figure 4 and Figure 5 set minimum s=250+2000/2+500/2=1500 µm or 1.5 mm and t=0.3 (SFH 5721)+0.25 (SFH 4053) = 0.55 mm for use in Equation 2.

Figure 4: Estimation of minimum spacing in set-up (250 µm)

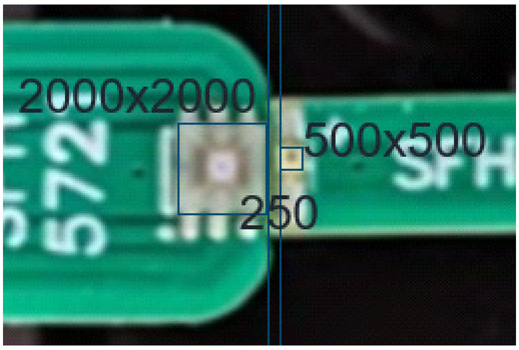

Figure 5: Package dimensions from SFH 5721 and SFH 4053 datasheets

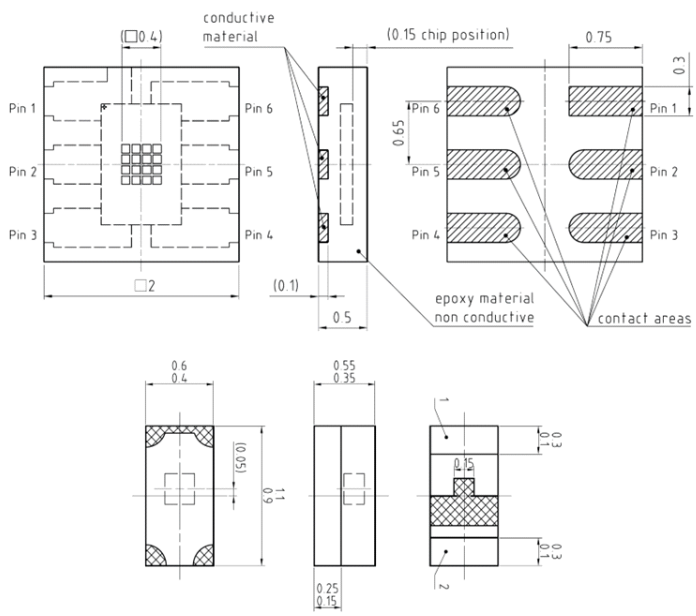

3.4 Specular (Aluminum tape) ceiling measurements data

Figure 6 shows the measured SFH 5721 counts and their one-ray model fit at various SFH 4053 bias currents as measured with a specular ceiling material (Aluminum). For discussion see section 3.6.

Figure 6: Specular measurement and fitted data at 0.25, 0.5, 0.8 and 2.4 mA SFH 4053 bias

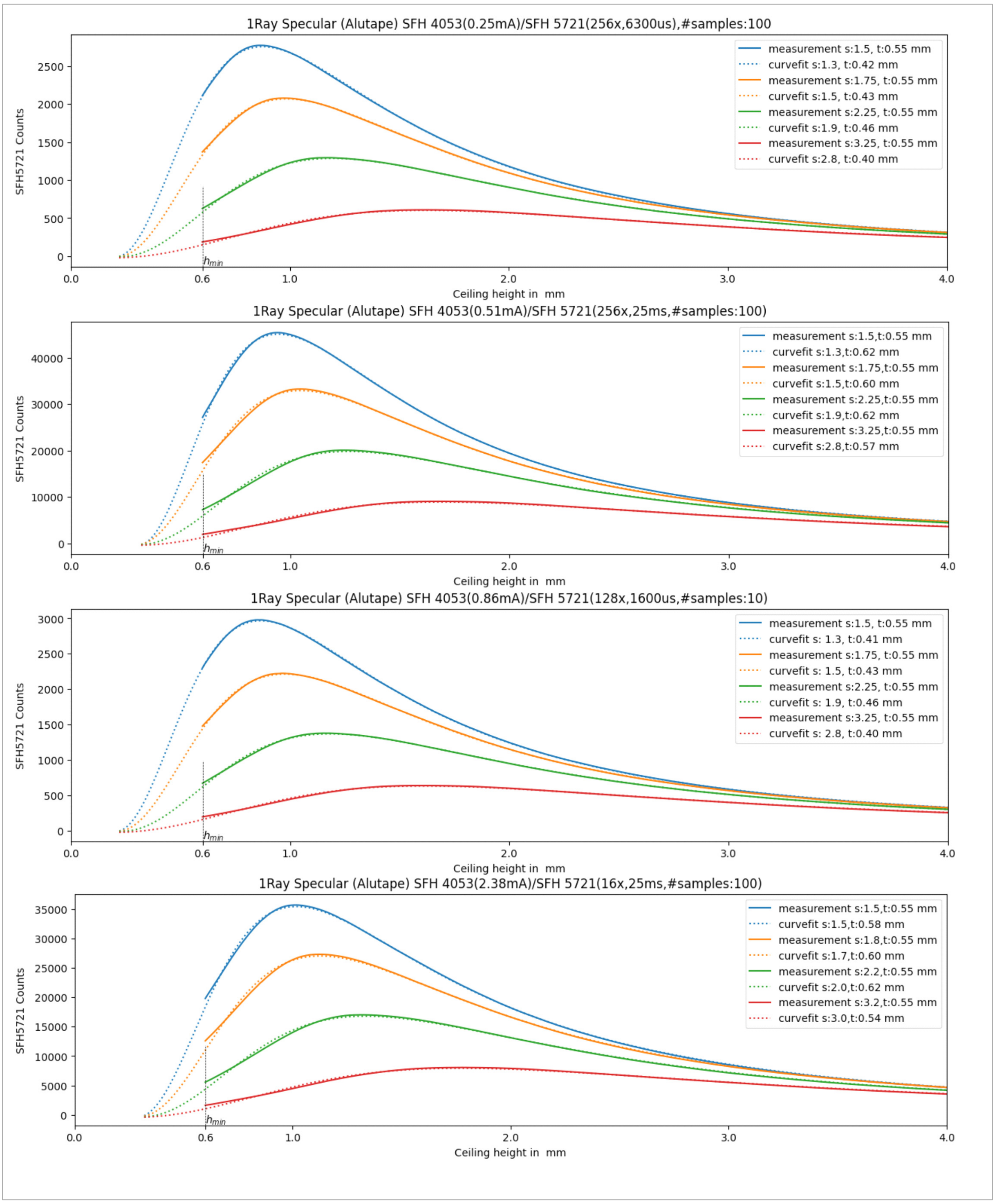

3.5 Diffuse (Teflon tape) ceiling measurement data

Figure 7 shows the measured SFH 5721 counts and their one-ray model fit for various SFH 4053 bias current settings as measured with a diffuse ceiling material (Teflon). For discussion see section 3.6.

Figure 7: Diffuse measurement and fitted data at 0.25, 0.5, 0.8 and 2.4 mA SFH 4053 bias

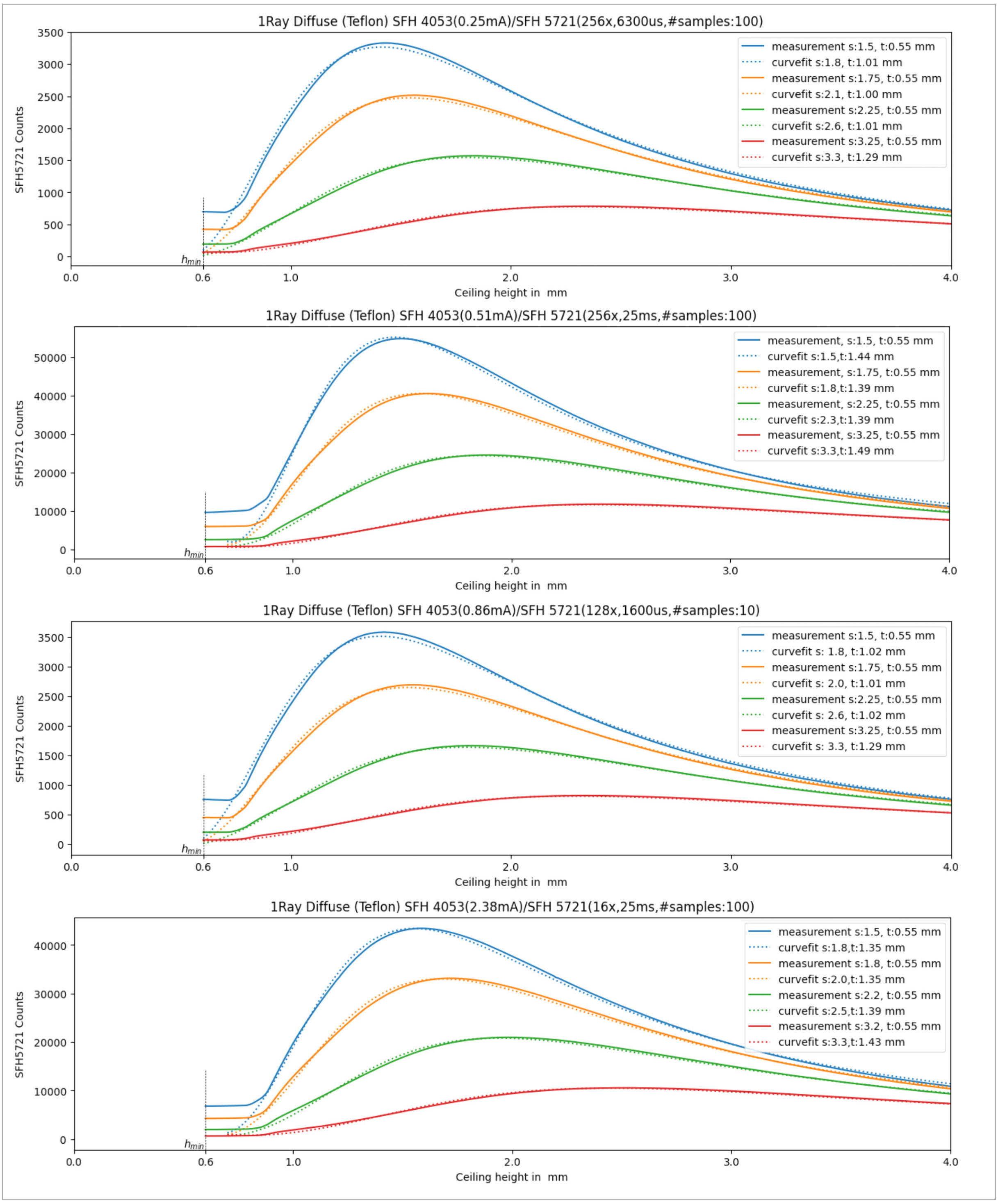

3.6 Discussion of measurement data

Sections 3.4 and 3.5 show the measurement data for specular and diffuse ceilings, respectively. Measured data was read into a Python Jupyter notebook and curve-fitted curve_fit routine imported from the Python scipy library.

All individual plots have titles with relevant parameters: the SFH 4053 bias current, the SFH 5721 gain and integration time setting, the reflective material used and the number of samples per data point. All of these are of influence on SFH 5721 counts output signal values on the y-axis. As the settings are identical between Aluminum and Teflon material settings, direct comparison of SFH 5721 output values is possible.

The x-axis is at the bottom of each plot, the ceiling height step is 10 µm, its range 0 – 4 mm. Per ceiling height 100 measurement samples were taken and averaged to one counts value and one counts standard deviation value.

Legends show the actual, fitted and delta values for s (spacing) and t (vertical offset). All plots show a close fit of Equation 2 with minor offset of the expected spacing and t values from section 3.3.

The plots allow several observations:

- Comparing SFH 5721 count values from Figure 6 to those of Figure 7 one sees that Teflon tape ceilings provide about a 15% higher reflectance than Aluminum tape ceilings
- As the model is derived from a single ray bouncing off a reflective ceiling in a mirror-like fashion, the specular data unsurprisingly have a closer fit to Equation 2 than the diffuse ones (where multiple emitter rays are contributing to ‘the reflected ray’)
- The curve-fitted values of s (the lateral spacing between the emitter and the detector) agree to a few tenths of millimeters. The curve-fitted values of t agree to about one tenth of a millimeter for the specular data.
- Measurements show the $\cos^2(\varphi)$ region has a steeper flank than the $1/d^2$ regions as explained in the text accompanying Figure 2
- The specular data doesn’t quite reach the zero counts level, as the height cannot be reduced below minimum height set by the highest component on the PCB (indicated by h_{min} in figures 6 and 7)
- We suggest that the multiple emitter ray integration and Lambertian redistribution effect of diffuse ceiling cause the plateau region at the lowest ceiling height levels that we see in Figure 7. Ignoring the plateau, diffuse ceilings can also be modeled adequately by Equation 2

3.7 Ceiling height uncertainty

3.7.1 Introduction

Figure 8: Ceiling height vs SFH 5721 counts uncertainty

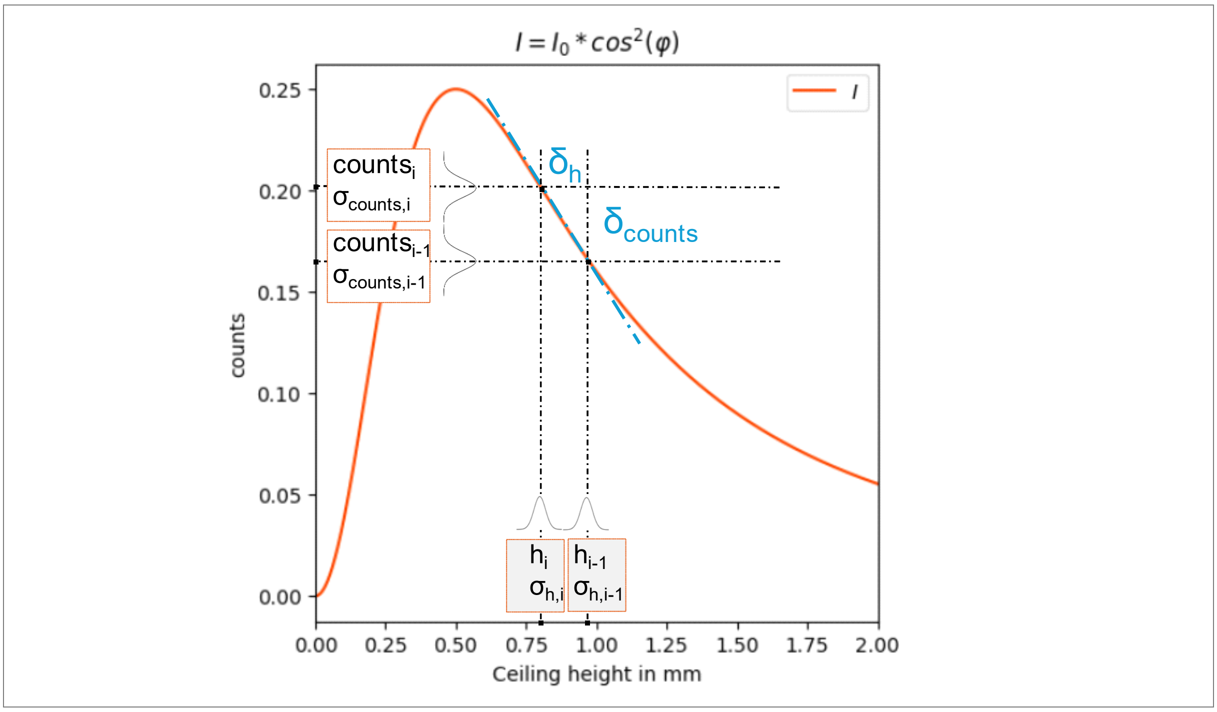

Figure 8 shows:

$$\sigma_h = \sigma_{Counts} \ldots \delta_h / \delta_{Counts}$$

Statistics textbooks tell us that when subtracting numbers, we need to sum their variances, so:

$$\sigma(Counts_i - Counts_{i-1}) = \sqrt{(\sigma^2_{Counts_i} + \sigma^2_{Counts_{i-1}})}$$

With this, calculation of the one sigma σ_h as a function of the measurement data points and their standard deviations is as in Equation 3.

Equation 3: Ceiling height uncertainty

$$\sigma_h = \sqrt{(\sigma^2_{Counts_i} + \sigma^2_{Counts_{i-1}})} \cdot \left| \frac{h_i - h_{i-1}}{Counts_i - Counts_{i-1}} \right|$$

We will use Equation 3 to calculate and plot σ_h from the measurement data in sections 3.7.2 through 3.7.5 for Aluminum and Teflon reflection materials, and we will show that even at low bias currents sub-micron ceiling height measurement accuracies can be achieved.

3.7.2 σ_h at 0.25 mA, gain 256x, t_{int} 6.3 ms

Figure 9: Ceiling height uncertainty at 0.25 mA SFH 4053 bias current, 6.3 ms t_{int}, 256x analog gain(1)

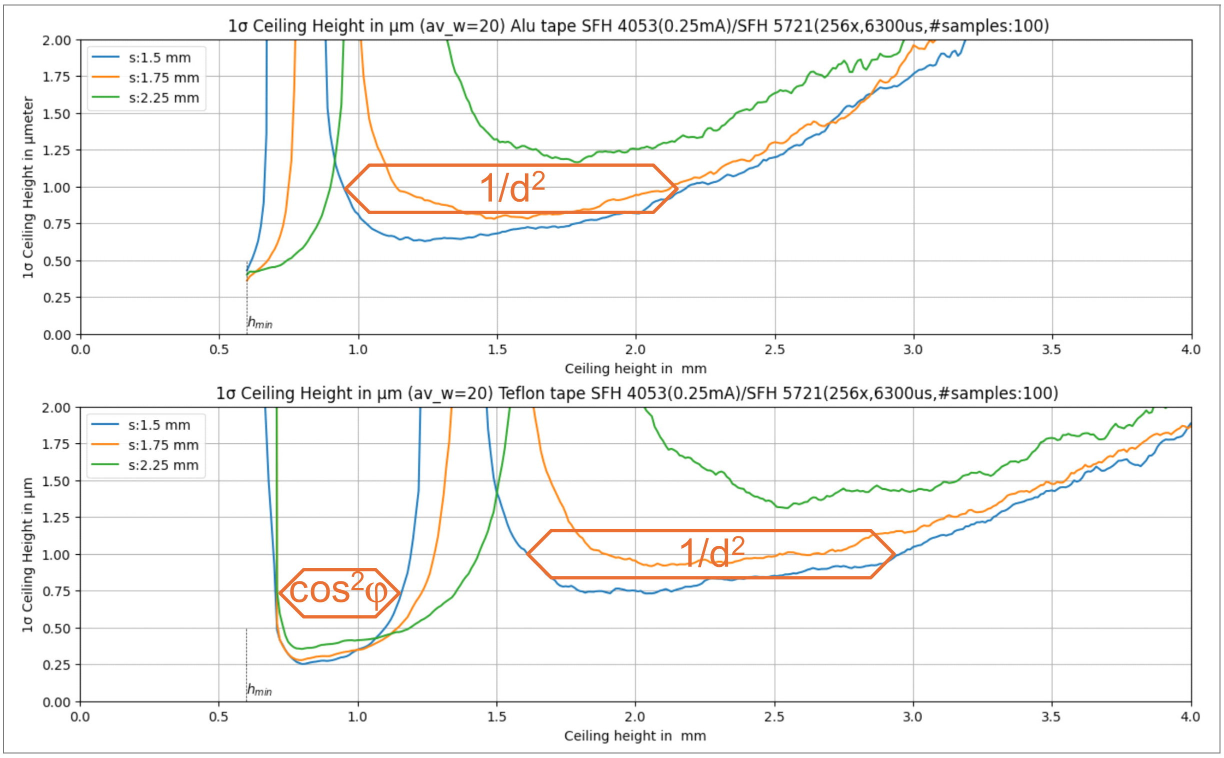

(1) Analog gain values are averaged 20 times for better readability

Figure 9's upper plot shows σ_h plot for specular (Aluminum) material, the lower plot shows σ_h for diffuse ceiling material (Teflon). Measurement results are averaged in a 20-data rolling window for better readability.

Figure 9 demonstrates, as the following pictures do, that smaller spacing values between emitter and detector lead to better uncertainty values (crosstalk subtracted).

The difference in σ_h curves between the Teflon and the Aluminum tape curves is striking, but both show that around 1-micron σ_h is achievable at 0.25 mA SFH 4053 bias current.

As we'll see at the other bias current settings, the plateau region as highlighted in the bottom plot of Figure 7 allows for a $\cos^2(\varphi)$ measurement window, but only for a diffuse ceiling material. Measurements show a slight improvement in σ_h at this $\cos^2(\varphi)$ window is possible at the cost of a smaller dynamic range (ceiling depression range; suggested by the width of the orange boxes).

One other thing to note is that a relatively short integration time of 6 ms is used for a measurement sequence which allows rapid system response times.

3.7.3 σ_h at 0.5 mA, gain 256x, t_{int} 25 ms

Figure 10: Ceiling height uncertainty at 0.5 mA SFH 4053 bias current, 25 ms t_{int}, 256x analog gain(1)

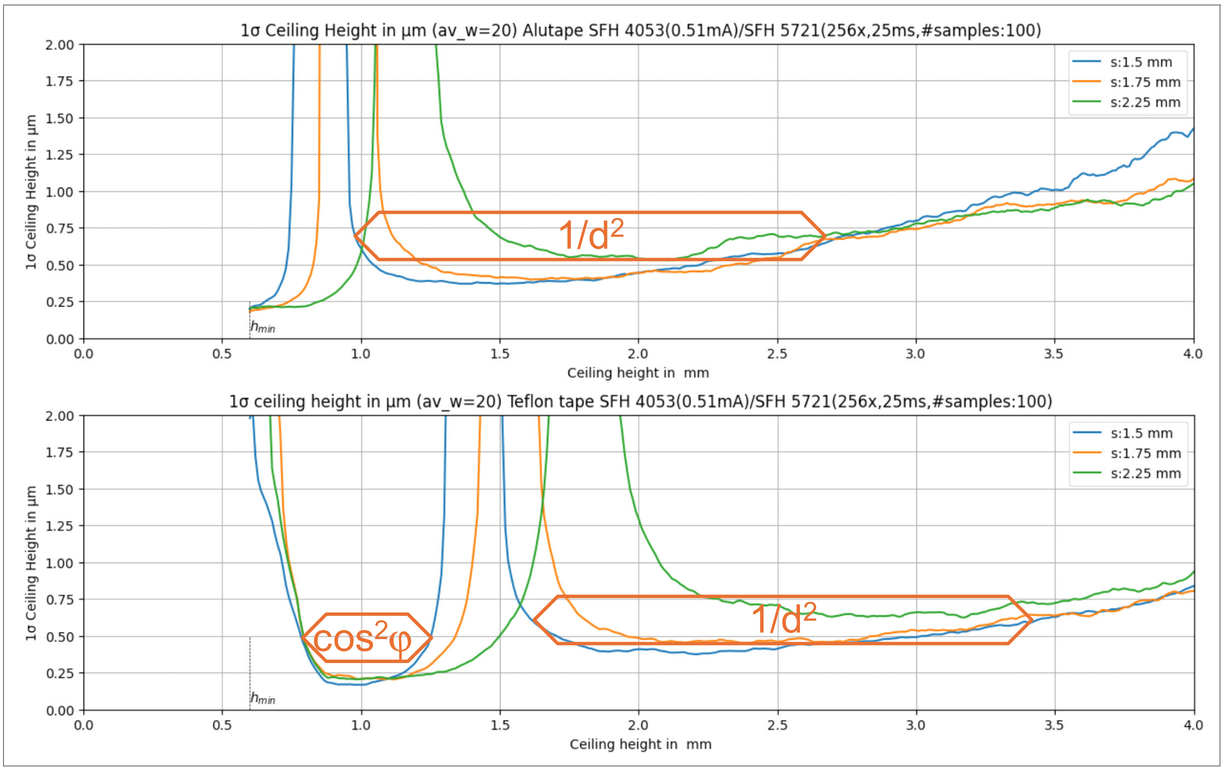

(1) Analog gain values are averaged 20 times for better readability

Higher bias current and a longer integration time of measurements in Figure 10 show markedly improved ceiling uncertainties and/or widening of the associated dynamic ranges.

25 ms is a relatively long integration time for a measurement sequence. Obviously, when needed for faster system responses, this can be shortened at the expense of worse ceiling height resolution.

3.7.4 σ_h at 0.8 mA, gain 128x, t_{int} 1.6 ms

Figure 11: Ceiling height uncertainty at 0.8 mA SFH 4053 bias current 1.6 ms t_{int}, 128x analog gain(1)

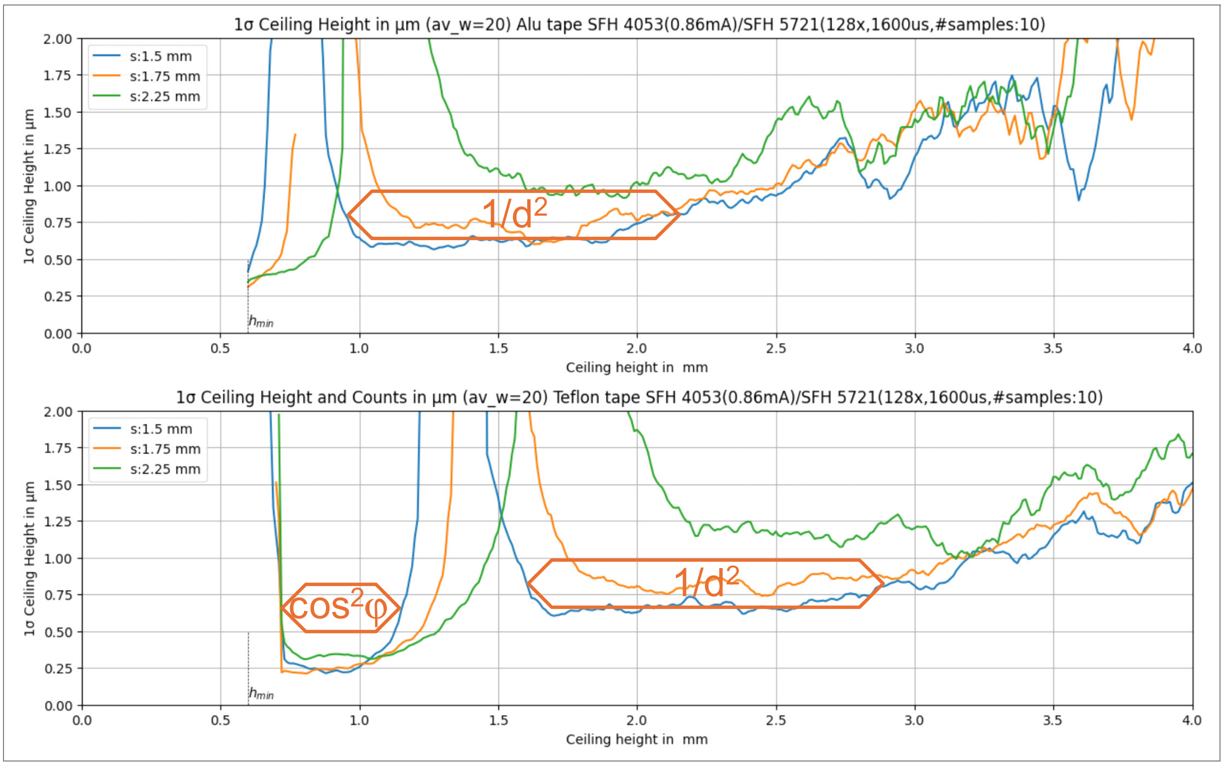

(1) Analog gain values are averaged 20 times for better readability

The further increased SFH 4053 bias current of the measurement of Figure 11 should allow equal or better ceiling height resolution from the previous pictures.

However, σ_h is negatively affected by other measurement settings like the lower SFH 5721 integration times (as low as 1.6 ms in these measurements) and by the lower SFH 5721 analog gain setting of 128x.

3.7.5 σ_h at 2.4 mA, gain 16x, t_{int} 25 ms

Figure 12: Ceiling height uncertainty at 2.4 mA SFH 4053 bias current 25 ms t_{int}, 16x analog gain(1)

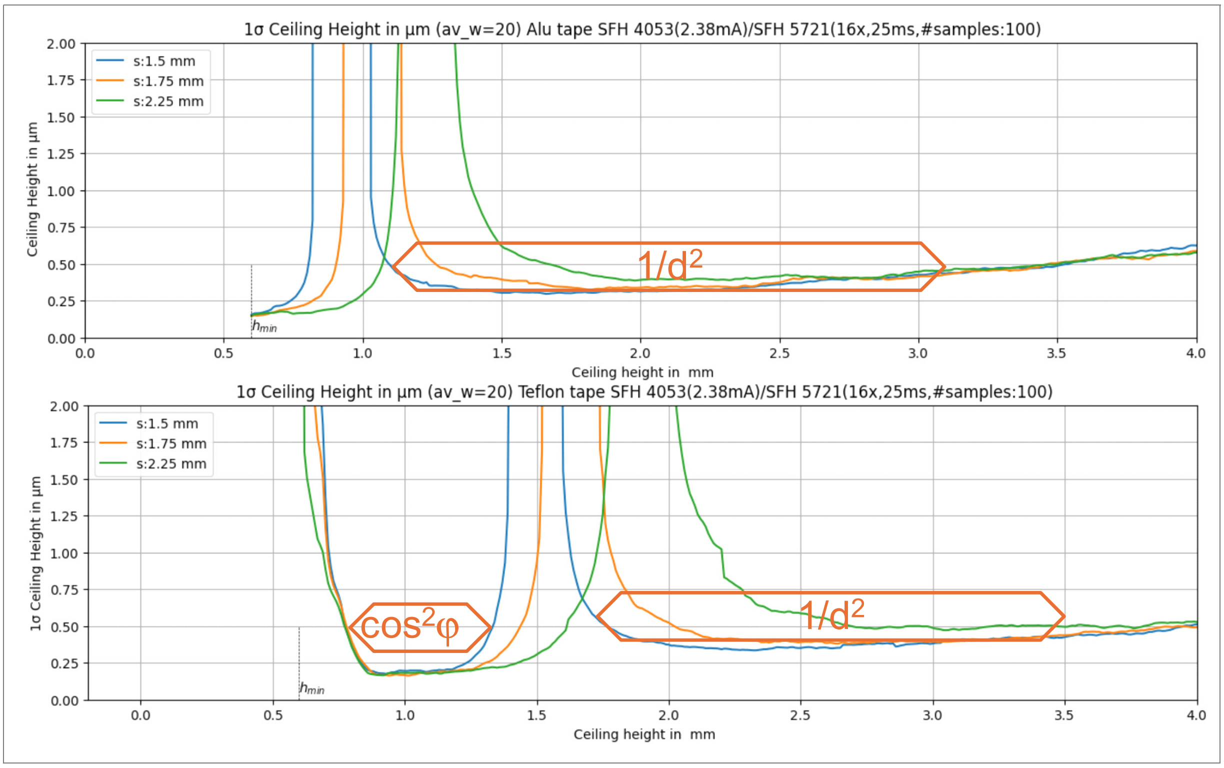

(1) Analog gain values are averaged 20 times for better readability

Using a 25 ms SFH 5721 integration time with a 2.4 mA SFH 4053 bias current as in Figure 12 shows that very low levels of ceiling height uncertainty and wide dynamic ranges are achievable.

3.7.6 Discussion of the σ_h results

In the last 4 sections we have tried to show the results of various SFH 4053 and SFH 5721 settings and their consequences in measurement results, they lead to a few interesting statements:

- SFH 5721 integration times, gain settings and SFH 4053 bias current all affect σ_h
- Smaller integration times can be compensated by higher bias currents
- Careful selection of gain setting to match emitter radiant intensity is key to low σ_h
- The ~15% higher SFH 5721 output of diffuse ceilings hardly translates in better σ_h
- Using a diffuse ceiling, there is a slight improvement in σ_h possible at the cost of lower dynamic range by measuring in the $\cos^2(\varphi)$ window
- Sub-micron σ_h values are achievable at mA bias and ceiling height below 3 mm

4 System statistical behavior

4.1 Probability measurements with fixed s, h and bias

To verify that we can use an approach of long continuous measurements during which we calculate mean values and signal to noise ratios, we measured sequences of ‘individual’ data samples of varying (but short) integration times and looked at their probability distribution.

Figure 13: Raw SFH 5721 counts measurements results at integration times from 0.2-3.2 ms

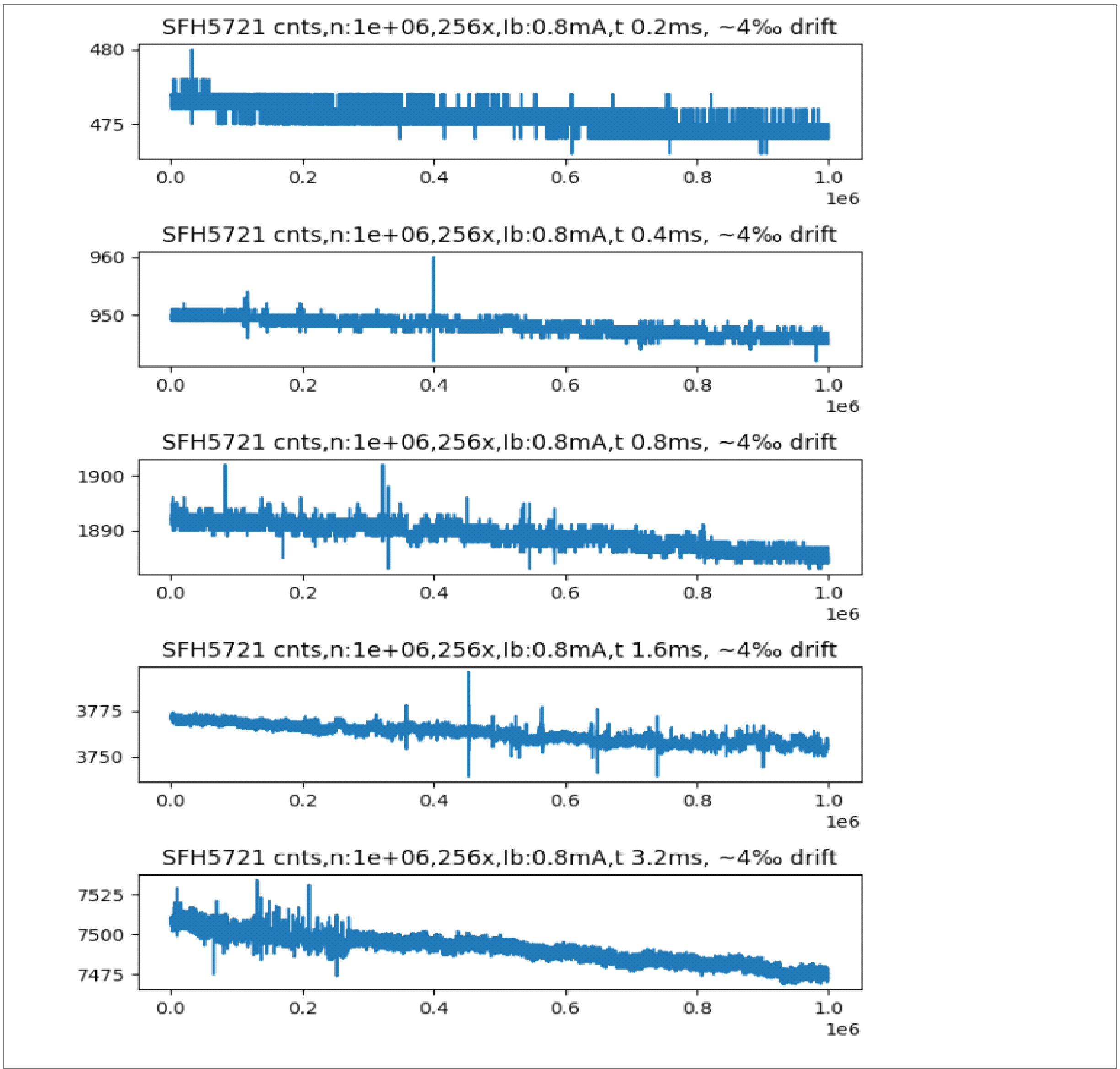

Figure 13 shows that during the long measurement times drift will occur in the order of parts of a percent (similar to values found in literature for the stability of a LED source).

After removal of the long-term drift and binning the measurement values, we get histograms as in Figure 14 that show an adequate fit to Gaussian probability density function when allowing for the limited statistics of the shorter integration times.

Figure 14: Data histograms and gaussian fit

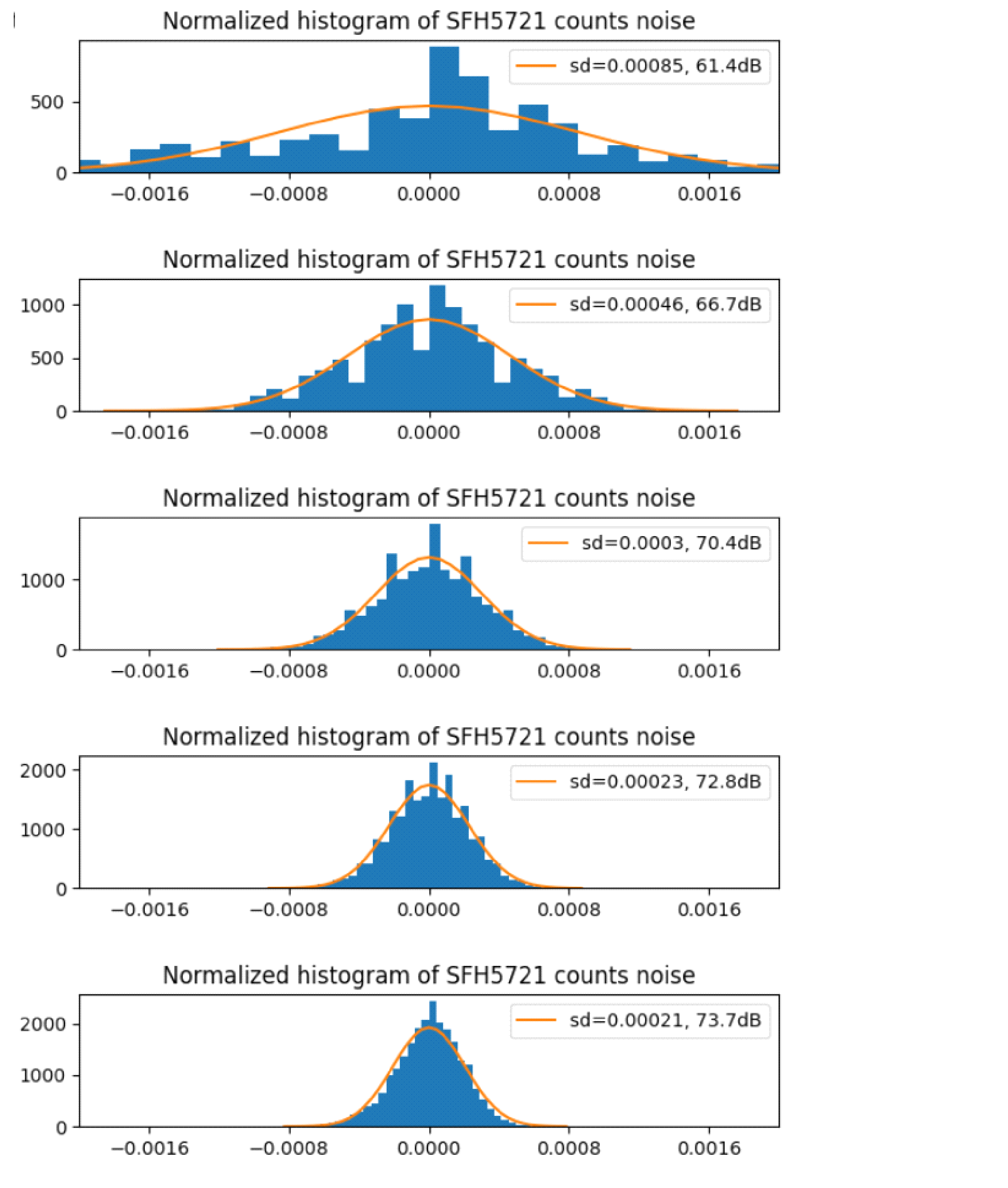

4.2 SFH 5721 σ_{Counts} as function of number of samples

Figure 15: SD development as function of SFH 5721 integration time

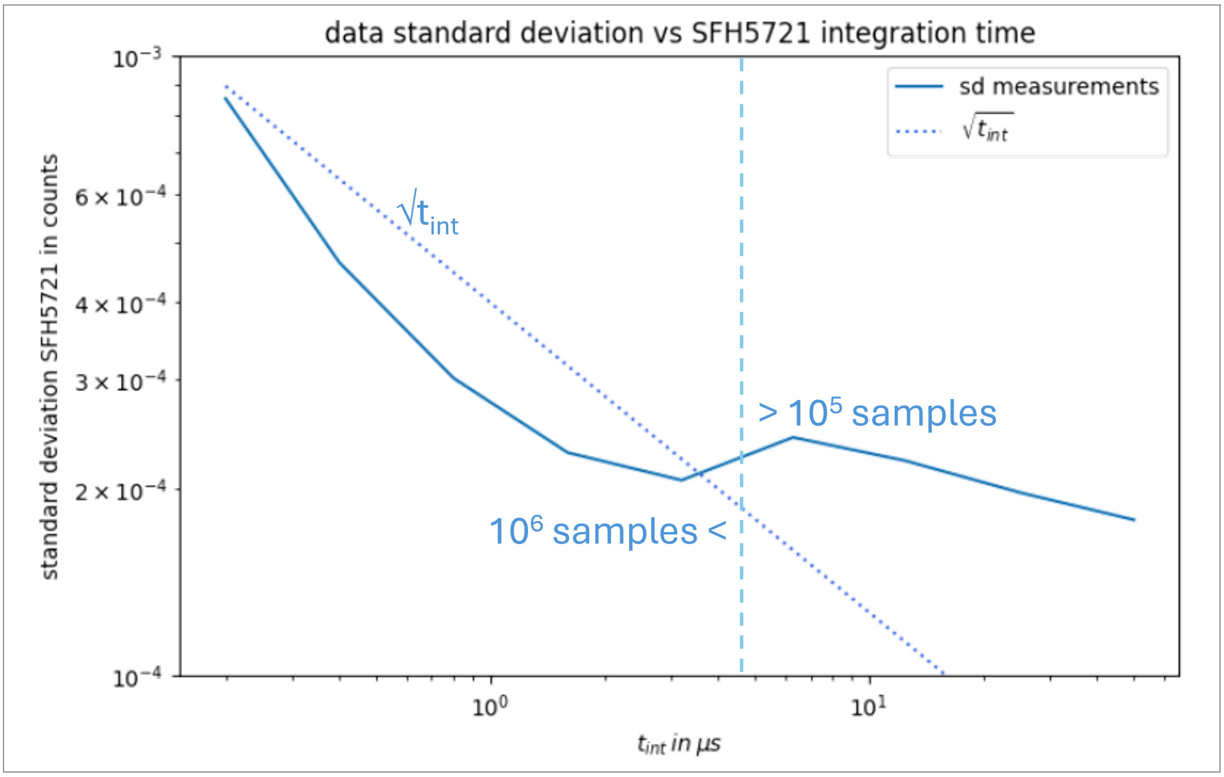

When we plot the relation between SFH 5721 σ_{Counts} and against its integration time, it becomes obvious that it does not fully follow the expected $1/\sqrt{t_{int}}$ curve.

We expect this $1/\sqrt{t_{int}}$ fit because the number of photons captured by the SFH 5721 detector increases linearly with its integration time as is evidenced by the count levels shown in Figure 13. Deviations from the fit are considered minor, and either caused by measurement accuracy, or a not completely Gaussian noise behavior of the SFH 5721 itself.

σ_{Counts} bottoms out at around 0.2×10^{-3}, equivalent to about 74 dB signal to noise ratio.

The discontinuity in the Figure 15 measurement curve is associated with the transition from 10^6 to 10^5 samples to accommodate higher integration times at reasonable measurement durations.

5 References

- SFH 4053
- SFH 5721
- Optical reflectance measurements for commonly used reflectors
- Low frequency noise and long-term stability of noncoherent light sources
- Standard deviation
- Jupyter
- scipy.optimize.curve_fit

6 Glossary

- **Count** – unitless SFH 5721 output value linear to the detector's irradiance in µW/cm²
- **Crosstalk** – light from the emitter resulting in a detector signal other than from the ceiling
- **Diffuse reflection** – incident ray reflected at many angles, ideally Lambertian
- **Lambertian emission** – emitted intensity proportional to the cosine of the angle φ between ray of interest and the surface's normal vector.
- **LED** – Light Emitting Diode: a semiconductor diode that emits light.
- **PCB** – Printed Circuit Board: a board connecting electronic components.
- **Reflectivity** – a measure of the ability of a surface to reflect light.
- **Specular reflection** – mirror like reflection, exit angle is equal to angle of incidence

7 Revision information

Changes to current revision v1-00	Page
Initial production version	

- Page and figure numbers for the previous version may differ from page and figure numbers in the current revision.
- Correction of typographical errors is not explicitly mentioned.

ABOUT ams OSRAM Group (SIX: AMS)

The ams OSRAM Group (SIX: AMS) is a global leader in optical solutions. By adding intelligence to light and passion to innovation, we enrich people's lives. This is what we mean by Sensing is Life. With over 110 years of combined history, our core is defined by imagination, deep engineering expertise and the ability to provide global industrial capacity in sensor and light technologies. Our around 24,000 employees worldwide focus on innovation across sensing, illumination and visualization to make journeys safer, medical diagnosis more accurate and daily moments in communication a richer experience. Headquartered in Premstaetten/Graz (Austria) with a co-headquarters in Munich (Germany), the group achieved over EUR 5 billion revenues in 2021. Find out more about us on https://ams-osram.com

For further information on our products please see the Product Selector and scan this QR Code.

Published by ams-OSRAM AG
Tobelbader Strasse 30, 8141 Premstaetten, Austria

Published by ams-OSRAM AG
Tobelbader Strasse 30,
8141 Premstaetten Austria
Phone +43 3136 500-0
ams-osram.com